Available online at www.sciencedirect.com
SCIENCE DIRECT®
International Journal of Mass Spectrometry 241 (2005) 197–204
International Journal of Mass Spectrometry
www.elsevier.com/locate/ijms

On the amphiphilic behavior of the hydrated proton: an ab initio molecular dynamics study

Srinivasan S. Iyengar[a,*], Tyler J.F. Day[b], Gregory A. Voth[b]

[a] *Department of Chemistry and Department of Physics, Indiana University, 800 E. Kirkwood Ave., Bloomington, IN 47405-7102, USA*
[b] *Department of Chemistry and Center for Biophysical Modeling and Simulation, 315 S. 1400 E. Rm. 2020, University of Utah, Salt Lake City, UT 84112-0850, USA*

Received 16 November 2004; accepted 1 December 2004
Available online 7 January 2005

Abstract

The ab initio atom-centered density matrix propagation (ADMP) method has been employed to study the dynamics of protonated water clusters of various sizes. An interesting result that hints at the possible amphiphilicity of the hydronium ion is detected. The hydrated proton tends to reside on the surface of the water clusters studied, with the lone pair on the protonated oxygen pointing "outwards" from the cluster. It is also noted that the hopping rate and average bonding topology in the local vicinity of the protonated species show a pronounced difference when treated with B3LYP and BLYP functionals. This is proposed to be on account of the potential for greater electronic exchange interactions in the vicinity of the positive charge.

Keywords: Ab initio molecular dynamics; ADMP; Atom-centered density matrix propagation; Protonated water clusters; Hydrophobicity; Amphiphilicity

1. Introduction

The structural and dynamical features of protonated and unprotonated water clusters [1–41] contribute significantly in biological [42–45], atmospheric [46,47] and condensed phase systems. Hence, these have been the subject of great experimental [3–12] and theoretical [2,19–40] interest. Early mass spectrometric studies [8,9,41] on protonated clusters revealed $H^+(H_2O)_{21}$ and $H^+(H_2O)_{31}$ to have greater stability as compared to clusters of similar sizes. Due to this fact, the well-studied $H^+(H_2O)_{21}$ species has often been referred to as a "magic number" cluster and its additional stability has been proposed as the reason for its greater abundance in the earth's stratosphere. This cluster has been of substantial interest to both experimentalists and theorists [1–3,8,9,41].

In this contribution, we have chosen to follow-up on our recent study [48] of the "directional hydrophobicity" of the hydrated proton. It was noted in [48] that a protonated species tends to reside on the surface of a water vacuum interface with its lone pairs directed away from the neighboring water molecules. The proposed reason for this effect as discussed in [48] is as follows. A single water molecule has on average four hydrogen bonds: two of these hydrogen bonds are donated from the oxygen atom to neighboring water molecules and one each is donated to the hydrogens from neighboring waters. When a water molecule gains an excess proton and becomes a hydronium, it gains a net positive charge. On average, the center of positive charge resides on the oxygen atom. Hence, while the hydrogen atoms in the hydronium retain their hydrogen bonds to the neighboring water molecules, the oxygen, on being the center of positive charge in a hydronium, is unable to support its hydrogen bond with any neighboring water molecule. Due to this reason, the solvation shell of a hydronium complex only comprises three water molecules on average. This reduction creates a lowering of the water density around the hydronium in the region directly in front of the lone pairs on the oxygen atom. Such a reduced density is entropically unfavorable to support in-

* Corresponding author. Tel.: +1 812 8561875; fax: +1 812 8558300.
E-mail address: iyengar@indiana.edu (S.S. Iyengar).

1387-3806/$ – see front matter © 2004 Elsevier B.V. All rights reserved.
doi:10.1016/j.ijms.2004.12.003

side the cluster, seemingly reminiscent of the hydrophobic effect. But if the hydronium were to be situated on the surface, with the lone pairs on the oxygen atom pointing "outwards", this reduction in density becomes a non-factor. In [48], we arrived at this conclusion based on the study of large water–vacuum interface systems using the computationally efficient second generation multi-state empirical valence bond (MS-EVB2) approach [49,50]. In the current paper, we have chosen to study this effect in smaller protonated water cluster systems using an ab initio molecular dynamics approach called atom-centered density matrix propagation (ADMP) [51–57]. While MS-EVB2 is extremely efficient and allows the proton to hop along an optimally located chain of water molecules, the inherent polarizability of the protonated environment and its constantly changing bonding topography renders itself attractive to an ab initio based study. Since ADMP does allow the use of accurate density functionals such as B3LYP and is efficient for reasonably large systems and since it has already been shown that ADMP can provide many properties in agreement with Born-Oppenhemier molecular dynamics [53,55,57], we have chosen to use this approach to further study protonated water clusters in this paper.

The paper is organized as follows: in Section 2 we briefly summarize the atom-centered density matrix propagation (ADMP) approach to ab initio molecular dynamics. More details can be found in [51–57]. In Section 3 the dynamical results are described; these involve ADMP studies conducted on protonated water clusters containing 31, 41 and 51 water molecules. All calculations are performed using B3LYP and BLYP density functionals using polarized double zeta gaussian basis functions. In Section 4 the conclusions are presented.

2. Computational methodology: brief overview of atom-centered density matrix propagation (ADMP)

In ADMP, the electronic structure, represented using the single particle electronic density matrix, is propagated simultaneously with the classical nuclei by a simple adjustment of the relative nuclear and electronic time-scales. It has been shown that this *fictitious* dynamics oscillates about the Born-Oppenheimer surface with controlable deviations [52,54] and agrees well with Born-Oppenheimer dynamics calculations [53,57]. ADMP has also been shown to be computationally superior to Born-Oppenheimer dynamics [53,55,57] and has been used to study several interesting applications [53,55,58]. Some well-documented advantages of ADMP [51–54] include: asymptotic *linear scaling of computation time with system size*, efficient use of reasonably larger time-steps for propagation, ability to use a range of accurate hybrid or gradient-corrected density functionals, and the ability to use chemically accurate basis-sets. These critical features of ADMP allow reliable study of reactive processes in systems with moderate (over 100) number of atoms [55]. The recently developed quantum mechanics/molecular mechanics (QM/MM) implementation of ADMP [55] facilitates the study of large biological systems. In addition, [57] contains a detailed exposition on the connections between the basis sets used in ADMP and the wavelet theory [59–62] of multi-resolution analysis. This is used in [57] to understand the effect of the time-dependent basis functions used in ADMP.

The ADMP equations of motion for the nuclei and density matrix are

$$\boldsymbol{M}\frac{\mathrm{d}^2\boldsymbol{R}}{\mathrm{d}t^2} = -\left.\frac{\partial E(\boldsymbol{R},\boldsymbol{P})}{\partial \boldsymbol{R}}\right|_{\boldsymbol{P}}, \tag{1}$$

$$\underline{\mu}^{1/2}\frac{\mathrm{d}^2\boldsymbol{P}}{\mathrm{d}t^2}\underline{\mu}^{1/2} = -\left[\left.\frac{\partial E(\boldsymbol{R},\boldsymbol{P})}{\partial \boldsymbol{P}}\right|_{\boldsymbol{R}} + \boldsymbol{\Lambda}\boldsymbol{P} + \boldsymbol{P}\boldsymbol{\Lambda} - \boldsymbol{\Lambda}\right], \tag{2}$$

where $\boldsymbol{R}$, $\boldsymbol{V}$ and $\boldsymbol{M}$ are the nuclear positions, velocities and masses, and $\boldsymbol{P}$, $\boldsymbol{W}$ and $\underline{\mu}$ are the density matrix, the density matrix velocity and the fictitious mass tensor for the electronic degrees of freedom. $\boldsymbol{\Lambda}$ is a Lagrangian multiplier matrix used to impose N-representability of the single particle density matrix. The energy, $E(\boldsymbol{R},\boldsymbol{P})$, is calculated using McWeeny purification, $\tilde{\boldsymbol{P}} = 3\boldsymbol{P}^2 - 2\boldsymbol{P}^3$,

$$\begin{aligned} E &= \mathrm{Tr}\left[\boldsymbol{h}'\tilde{\boldsymbol{P}}' + \frac{1}{2}\boldsymbol{G}'(\tilde{\boldsymbol{P}}')\tilde{\boldsymbol{P}}'\right] + E_{\mathrm{xc}} + V_{\mathrm{NN}} \\ &= \mathrm{Tr}\left[\boldsymbol{h}\tilde{\boldsymbol{P}} + \frac{1}{2}\boldsymbol{G}(\tilde{\boldsymbol{P}})\tilde{\boldsymbol{P}}\right] + E_{\mathrm{xc}} + V_{\mathrm{NN}}. \end{aligned} \tag{3}$$

Here, $\boldsymbol{h}'$ is the one electron matrix in the non-orthogonal Gaussian basis and $\boldsymbol{G}'(\tilde{\boldsymbol{P}}')$ is the two electron matrix for Hartree–Fock calculations, but for DFT it represents the Coulomb potential. The term E_{xc} is the DFT exchange-correlation functional (for Hartree–Fock $E_{\mathrm{xc}} = 0$), while V_{NN} represents the nuclear repulsion energy. In the orthonormal basis, these matrices are $\boldsymbol{h} = \boldsymbol{U}^{-\boldsymbol{T}}\boldsymbol{h}'\boldsymbol{U}^{-1}$, etc., where the overlap matrix for the non-orthogonal Gaussian basis, $\boldsymbol{S}'$, is factorized to yield $\boldsymbol{S}' = \boldsymbol{U}^{\boldsymbol{T}}\boldsymbol{U}$. There are a number of choices for the transformation matrix $\boldsymbol{U}$, e.g., $\boldsymbol{U}$ can be obtained from Cholesky decomposition [63] of $\boldsymbol{S}'$ or $\boldsymbol{U} = \boldsymbol{S}'^{1/2}$ for Löwdin symmetric orthogonalization. The density matrix in the orthonormal basis, $\boldsymbol{P}$, is related to the density matrix in the non-orthogonal Gaussian basis, $\boldsymbol{P}'$, by $\boldsymbol{P} \equiv \boldsymbol{U}\boldsymbol{P}'\boldsymbol{U}^{\boldsymbol{T}}$. The gradient terms involved in the equations of motion are

$$\left.\frac{\partial E(\boldsymbol{R},\boldsymbol{P})}{\partial \boldsymbol{P}}\right|_{\boldsymbol{R}} = 3\boldsymbol{F}\boldsymbol{P} + 3\boldsymbol{P}\boldsymbol{F} - 2\boldsymbol{F}\boldsymbol{P}^2 - 2\boldsymbol{P}\boldsymbol{F}\boldsymbol{P} - 2\boldsymbol{P}^2\boldsymbol{F}, \tag{4}$$

where $\boldsymbol{F}$ is the Fock matrix and in the non-orthogonal basis:

$$\boldsymbol{F}'_{\nu,\sigma} \equiv \boldsymbol{h}'_{\nu,\sigma} + \boldsymbol{G}'(\tilde{\boldsymbol{P}}')_{\nu,\sigma} + \frac{\partial E_{\mathrm{xc}}}{\partial \boldsymbol{P}'}, \tag{5}$$

while the orthogonal basis Fock matrix is $\boldsymbol{F} = \boldsymbol{U}^{-T}\boldsymbol{F}'\boldsymbol{U}^{-1}$. The nuclear gradients are

$$\left.\frac{\partial E}{\partial \boldsymbol{R}}\right|_{\boldsymbol{P}} = \left\{ \mathrm{Tr}\left[\frac{\mathrm{d}\boldsymbol{h}'}{\mathrm{d}\boldsymbol{R}}\tilde{\boldsymbol{P}}' + \frac{1}{2}\left.\frac{\partial \boldsymbol{G}'(\boldsymbol{P}')}{\partial \boldsymbol{R}}\right|_{\boldsymbol{P}'}\tilde{\boldsymbol{P}}'\right] - \mathrm{Tr}\left[\boldsymbol{F}'\tilde{\boldsymbol{P}}'\frac{\mathrm{d}\boldsymbol{S}'}{\mathrm{d}\boldsymbol{R}}\tilde{\boldsymbol{P}}'\right] + \left.\frac{\partial E_{\mathrm{xc}}}{\partial \boldsymbol{R}}\right|_{\boldsymbol{P}} + \frac{\partial V_{\mathrm{NN}}}{\partial \boldsymbol{R}}\right\} + \mathrm{Tr}\left[[\tilde{\boldsymbol{P}}, \boldsymbol{F}]\left(\tilde{\boldsymbol{Q}}\frac{\mathrm{d}\boldsymbol{U}}{\mathrm{d}\boldsymbol{R}}\boldsymbol{U}^{-1} - \tilde{\boldsymbol{P}}\boldsymbol{U}^{-T}\frac{\mathrm{d}\boldsymbol{U}^{T}}{\mathrm{d}\boldsymbol{R}}\right)\right], \tag{6}$$

where $\tilde{\boldsymbol{Q}} \equiv \boldsymbol{I} - \tilde{\boldsymbol{P}}$. Note that as the commutator $[\tilde{\boldsymbol{P}}, \boldsymbol{F}] \rightarrow 0$, the nuclear forces tend to those used in the standard Born-Oppenheimer MD [51,54,64]. However, in ADMP, the magnitude of the commutator $[\tilde{\boldsymbol{P}}, \boldsymbol{F}]$ is non-negligible and hence the general expression for the nuclear gradients [51,54] in Eq. (6) is used.

The dynamics obtained in ADMP is fictitious since the density matrix is directly propagated classically using the N-representability Lagrangian constraints. The accuracy and efficiency of the scheme is governed by the choice of the fictitious mass tensor, $\underline{\mu}$; hence, one must be aware of the limits on this quantity. We have derived two criteria [52,54] that place bounds on the choice of the fictitious mass. Firstly, the choice of the fictitious mass determines the magnitude of the commutator $[\tilde{\boldsymbol{P}}, \boldsymbol{F}]$ thus determining the extent of deviation from the Born-Oppenheimer surface [54]:

$$||[\boldsymbol{F}, \boldsymbol{P}_{\mathrm{approx}}]||_{\mathrm{F}} \geq \frac{1}{||[\boldsymbol{P}_{\mathrm{approx}}, \boldsymbol{W}]||_{\mathrm{F}}}\left|\mathrm{Tr}\left[\boldsymbol{W}\underline{\boldsymbol{\mu}}^{1/2}\frac{\mathrm{d}\boldsymbol{W}}{\mathrm{d}t}\underline{\boldsymbol{\mu}}^{1/2}\right]\right|, \tag{7}$$

where $||[\ldots]||_{\mathrm{F}}$ is the Frobenius norm [63,65] of the commutator and is defined as $||A||_{\mathrm{F}} = \sqrt{\sum_{i,j} A_{i,j}^2}$. Secondly, the rate of change of the fictitious kinetic energy,

$$\frac{\mathrm{d}\mathcal{H}_{\mathrm{fict}}}{\mathrm{d}t} = \mathrm{Tr}\left[\boldsymbol{W}\underline{\boldsymbol{\mu}}^{1/2}\frac{\mathrm{d}^2\boldsymbol{P}}{\mathrm{d}t^2}\underline{\boldsymbol{\mu}}^{1/2}\right] = -\mathrm{Tr}\left[\boldsymbol{W}\left(\left.\frac{\partial E(\boldsymbol{R}, \boldsymbol{P})}{\partial \boldsymbol{P}}\right|_{\boldsymbol{R}} + \boldsymbol{\Lambda}\boldsymbol{P} + \boldsymbol{P}\boldsymbol{\Lambda} - \boldsymbol{\Lambda}\right)\right], \tag{8}$$

is required to be *bounded and oscillatory* and this again is determined by the choice of fictitious mass tensor. Eq. (8) represents the instantaneous deviation of the ADMP trajectory from adiabatic behavior. Although the ADMP trajectory does not exactly remain on the Born-Oppenheimer surface (due to no SCF convergence), it is required that long time averages provide similar results as in Born-Oppenheimer molecular dynamics. This leads to the requirement that the quantity in Eq. (8) be an oscillatory function such that its average value is small. There is, however, also a second condition enforced by Eq. (8), and this is the requirement that the instantaneous value of the quantity in Eq. (8) should be bounded and less than some pre-defined threshold. Clearly the latter is a stronger condition and *both conditions must be met in order to maintain adiabatic behavior*. Please see [52,54] for a detailed exposition of these requirements. Furthermore, note that the right hand side of Eq. (8) is equal to the numerator in Eq. (7) which leads to the fact that $\mathrm{d}\mathcal{H}_{\mathrm{fict}}/\mathrm{d}t$ does in fact influence the value of the commutator, and hence deviations from the Born-Oppenheimer surface. One must monitor the quantities in Eqs. (7) and (8) to ascertain that the ADMP dynamics is physically consistent. In all applications studied to date [51–53,55,58,66] these conditions are satisfied thus yielding a computationally efficient and accurate approach to model dynamics on the Born-Oppenheimer surface.

Current implementation of the ADMP approach has been found to be computationally superior to Born-Oppenheimer dynamics [53,57] by over a factor of two, for fixed total simulation time. This is true for cases where the SCF convergence is not too difficult when using Born-Oppenheimer dynamics. For difficult cases such as transition metals, ADMP is expected to be further preferred.

3. Results and discussion

In ADMP the choice of basis set and density functionals is critical. To exercise proper choice, a detailed analysis was conducted using a variety of basis functions and density functionals (such as B3LYP, BLYP and BPBE) for the water dimer system, with and without basis-set superposition error [57]. Based on these results, the B3LYP density functional was chosen for all ADMP simulations. (Some calculations were also performed using BLYP, for comparison.) A time step of 0.25 fs in ADMP, and valence fictitious mass of 180 a.u., along with a tensorial mass-weighting scheme [52], were employed in all calculations. All ADMP simulations were performed under constant temperature, which was enforced by velocity scaling. The instantaneous temperature was calculated assuming the equipartition theorem, and it was found that approximately 95% of the states were within 10 K from the target temperature, which was considered satisfactory. All calculations were performed using the Gaussian series of electronic structure codes [67].

Protonated water clusters of various sizes: $H^+(H_2O)_{31}$, $H^+(H_2O)_{41}$ and $H^+(H_2O)_{51}$ were studied using ADMP. While the dynamics of the 31-mer was studied at 200 K and 300 K using B3LYP and BLYP functionals, the 41-mer and 51-mer clusters were only studied at 300 K using the B3LYP functional. The starting geometries in all cases had the proton fully solvated in the center of the cluster. The position of the most protonated water molecule at every simulation step was tracked through the dynamics. The most protonated water molecule for each simulation step was defined as being located on the oxygen atom having the minimum value of $|OH_1 - OH_3|$, where OH_1 is the shortest O–H distance for a given oxygen and OH_3 is the third shortest O–H dis-

tance for the same oxygen. The oxygen that has the minimum value for this parameter, is the one that is most hydronium-like (the pivot oxygen [24]) for the given time step. For some cases, it was found that more than one oxygen atom had a small value for the parameter in $|OH_1 - OH_3|$, implying the presence of a Zundel ($H_5O_2^+$) [17], Eigen ($H_9O_4^+$) [15,16] or similar delocalized protonated complex. However, even in these cases, there was always one oxygen that had a value of this parameter lower than other oxygens. This is clearly seen from the presence of two separated peaks in Fig. 1(a), where we present the distribution of the $|OH_1 - OH_3|$ for the $H_3O^+(H_2O)_{30}$ system. The larger height of the peak close to 1 Å in Fig. 1(a) implies that a great majority of the waters are unprotonated. (The peak close to 1 Å distance in Fig. 1(a) corresponds to the difference between OH_1 and OH_3 for an unprotonated water molecule.) The peak close to 0 in Fig. 1 is due to the protonated species and has a much lower intensity since on average there are 30 times more unprotonated water molecules as compared to protonated in the 31-mer. Note the close similarity in distribution for B3LYP and BLYP functionals. A further degree of sophistication in locating a "center of excess charge" could be achieved by performing a weighted average of the inverse of $|OH_1 - OH_3|$ over the positions of all (or some) oxygens in the cluster. This was, however, not found to be necessary in the current study.

Since ADMP is an ab initio simulation technique it allows a dynamical change in the bonding topology surrounding the protonated species and the subsequent transport of the excess proton along an optimal conformation of water molecules consistent with the Grotthuss mechanism of proton-transfer [13–18]. As a result, the most protonated oxygen is found for every given nuclear configuration in the dynamics. We then study the evolution of the protonated species from the center of the cluster. In Fig. 2 we present the time-evolution of the size of the cluster, and the number of water molecules on the surface side of the most protonated oxygen but inside the solid angle cone defined by the most protonated oxygen, the center of the cluster and a disk of radius 3 Å centered at the most protonated oxygen and perpendicular to the line joining the most protonated oxygen (represented as N_{out}). The cluster size in Fig. 2 is defined as the distance of the farthest oxygen from the cluster center. The data is shown for $H^+(H_2O)_{31}$, $H^+(H_2O)_{41}$ and $H^+(H_2O)_{51}$ clusters. The results are provided for both B3LYP and BLYP density functionals for the 31-mer and B3LYP for the 41-mer and 51-mer. The discontinuities in the plot for N_{out} are due to proton hops occuring as per the Grotthus mechanism [13] and the fact that N_{out} is always a natural number. It is clear from the Fig. 2 that the number of water molecules on the surface side of the most protonated oxygen decreases as the simulation progresses for all calculations. Hence, the protonated species accomplishes a sequence of hops that takes it closer to the surface of the cluster. Furthermore, after reaching the surface, the protonated species traverses the hydrogen bond network existing among the surface water molecules, thus continuing its presence on the surface. One important feature in all simulations was that, after the protonated species migrated to the surface of the cluster, the lone pair on the most protonated oxygen atom was always directed outwards from the cluster. This aspect suggests the important concept that the protonated species in water clusters has "hydrophobic" and "hydrophilic" sites; the hydrophobic region being in the vicinity of the lone pair on the oxygen atom. This is completely consistent with our earlier study in [48], where it was noted that the hydronium has a "hydrophobic" region which is located close to the lone pair on the oxygen. In Fig. 3 we present a representative structure from the ADMP simulation of $H_3O^+(H_2O)_{30}$ using the B3LYP functional. The Zundel complex on the surface is clearly represented using a dark shaded area. It is further interesting to note that the

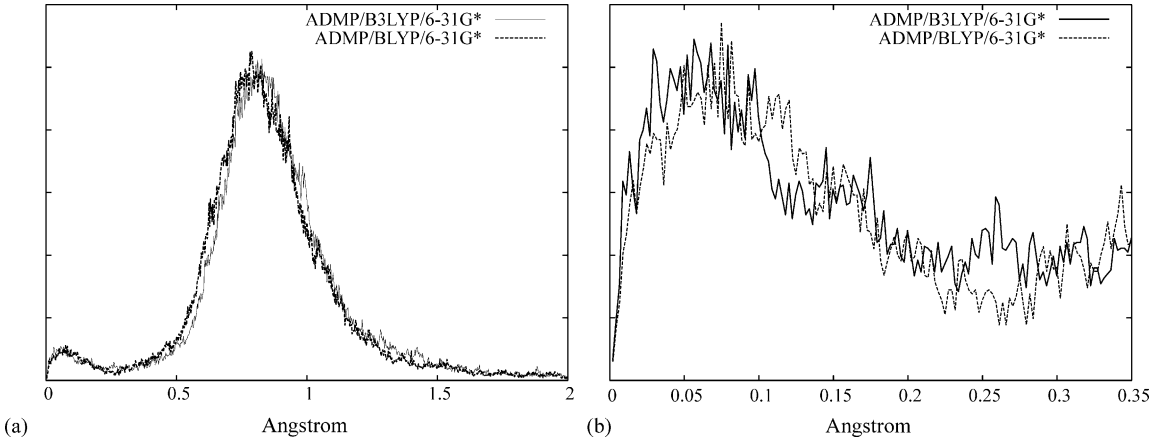

Fig. 1. Distribution of the parameter $|OH_1 - OH_3|$ which is used to detect the most protonated (or pivot) oxygen in the cluster, during the ADMP dynamics of the $H_3O^+(H_2O)_{30}$ system. For a perfect hydronium this parameter is expected to be close to 0 Å while for a perfectly unprotonated water this parameter is expected to be close to 1 Å. Consequently two separated peaks are seen; the peak close to zero is enhanced in (b). The reason for the low intensity of the peak close to zero is due to the fact that there are roughly 30 times more unprotonated water molecules in the cluster as compared to protonated water molecules. B3LYP and BLYP show similar distributions.

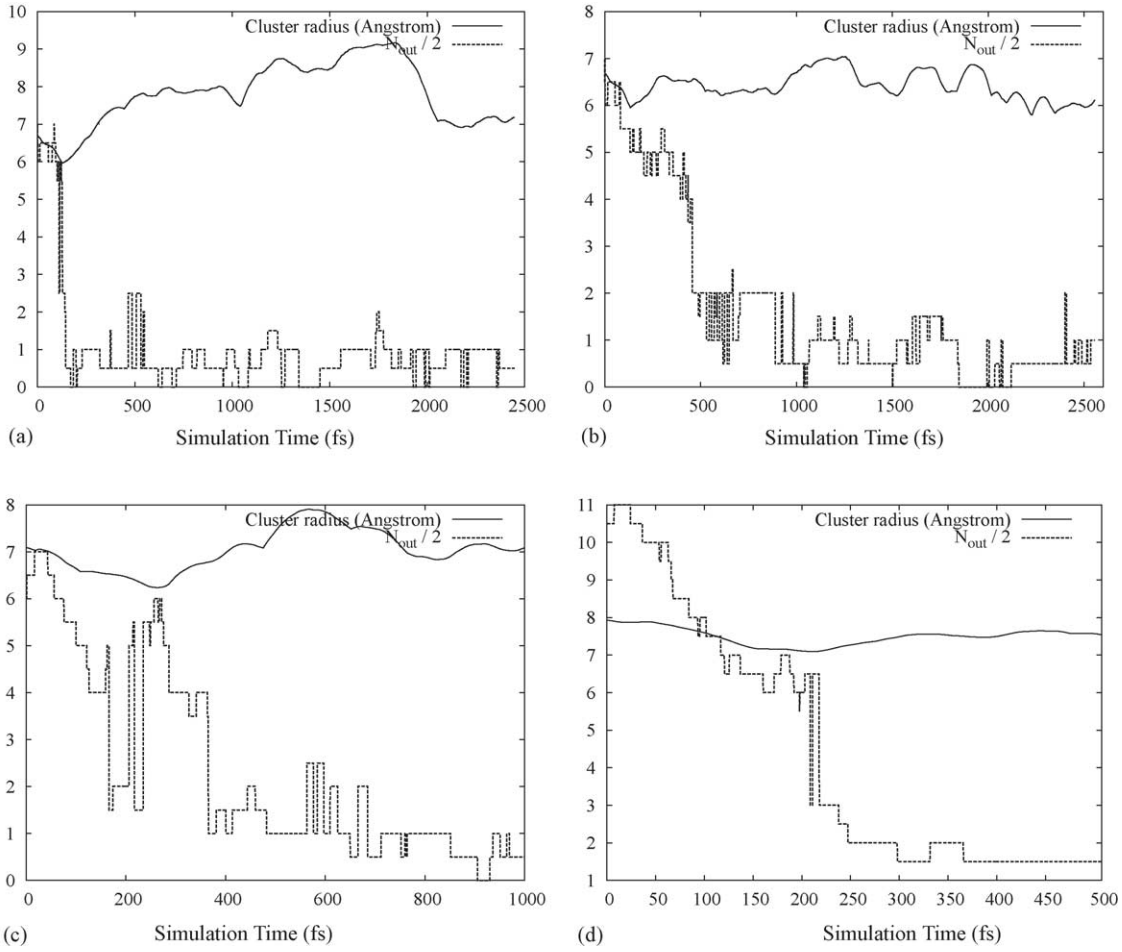

Fig. 2. Time-evolution of the protonated state for (a) the $H^+(H_2O)_{31}$ cluster at BLYP/6-31G* level of DFT theory, (b) the $H^+(H_2O)_{31}$ cluster at B3LYP/6-31G*, (c) the $H^+(H_2O)_{41}$ cluster at B3LYP/6-31G* and (d) the $H^+(H_2O)_{51}$ cluster at B3LYP/6-31G*. The quantity N_{out} is the number of water molecules on the surface side of the protonated species (H_3O^+, $H_5O_2^+$, $H_9O_4^+$ or similar delocalized species). In all cases the number of water molecules on the surface side of the most protonated species goes down with simulation time. The temperature for all data shown in this figure is 300 K.

lone pairs on the Zundel oxygens are directed outwards from the cluster.

While the qualitative results are similar for both B3LYP and BLYP simulations, there are important quantitative differences. In the case of BLYP, the oxygen gets to the surface within the first 100 fs, but it takes almost 1 ps in B3LYP to get to the surface. (The initial conditions were identical for both simulations.) This provides a basis for some comparison between the behavior of the two exchange-correlation functionals. To understand this difference we investigate the behavior of the radial distribution function between the most protonated oxygen (corresponding to the minimum value of $|OH_1 - OH_3|$) and other oxygens for the B3LYP and BLYP cases. Our results are shown in Fig. 4(a). The BLYP functional shows equal probability at both ca. 2.45 Å (the Zundel, $H_5O_2^+$, O*–O distance [24], where O* is the most-protonated or pivot oxygen) and at ca. 2.55 Å (the Eigen, $H_9O_4^+$ O*–O distance [24]), while the B3LYP functional prefers the Zundel over Eigen arrangement by over a factor of 2. Hence, the proton in the BLYP calculation is, on average, delocalized over a larger number of water molecules (on account of the larger $H_9O_4^+$ probability) as compared to that in the B3LYP calculation. This result may also be expected from previous results [28] which show that the proton transfer barriers in the BLYP functional are lower than those obtained from B3LYP. A lower proton transfer barrier leads to greater probability of sharing of the proton and hence a greater degree of delocalization. This larger delocalization then results in a faster transport of the proton to the surface in the case of BLYP. Furthermore, it has been noted previously [24] that the rate of proton transfer in a water chain is directly related to the ratio of Eigen to Zundel populations. Here, for the BLYP functional this ratio is closer to unity, which also explains the faster hopping rate for BLYP. In Fig. 4(b) we compare the radial distribution function between all other oxygens for B3LYP and BLYP. Interestingly these results are very similar. Hence, it is only the local properties of the cluster around the hydronium ion that are affected by the choice of B3LYP and BLYP functionals.

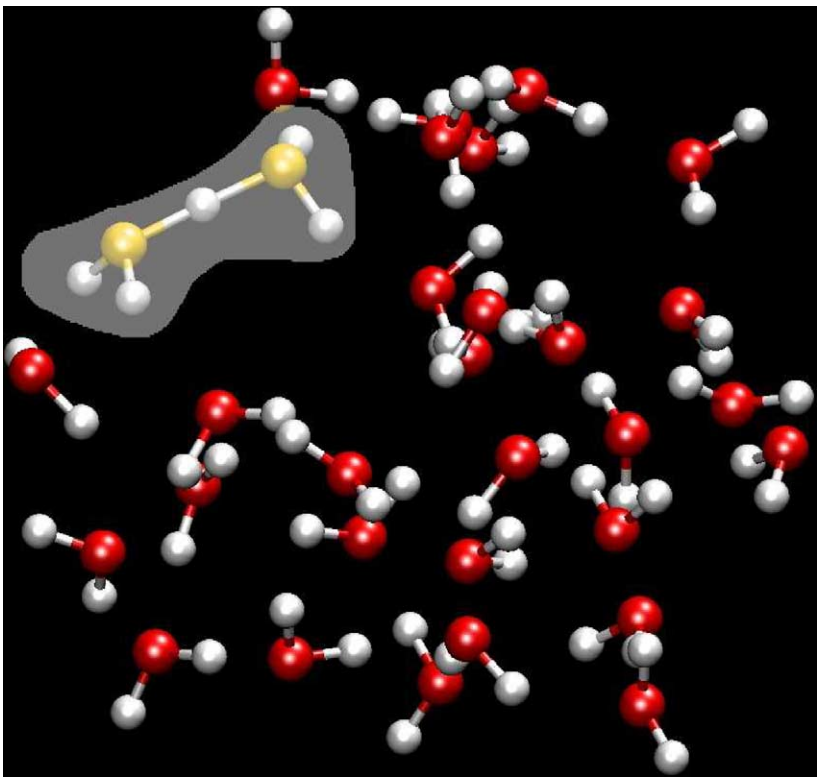

Fig. 3. A representative structure from the ADMP-B3LYP/6-31G* simulation of the $(H_2O)_{30}H_3O^+$ cluster. The Zundel ion on the surface is shown using the dark shaded area. The water molecules hydrogen bonded to the Zundel are shown using the light shaded area.

This aspect of faster hopping in BLYP was also noted during our earlier QMMM/ADMP study of the Gramicidin-A ion channel in [55]. Similar Eigen and Zundel populations were found for the case of BLYP. However, in that case, the system is essentially a water-wire inside a Gramicidin-A ion-channel, and hence the third hydrogen bond donated to a protonated species in the wire is due to the Gramicidin-A backbone carbonyl groups. This similarity in results between the water-wire found in Gramicidin-A and the water cluster studied here leads us to the following conclusion: the presence of the positive charge leads to a greater presence of the electrons in the close vicinity of the protonated species leading to a greater propensity for exchange interactions thus making a functional rich in exchange (such as B3LYP)

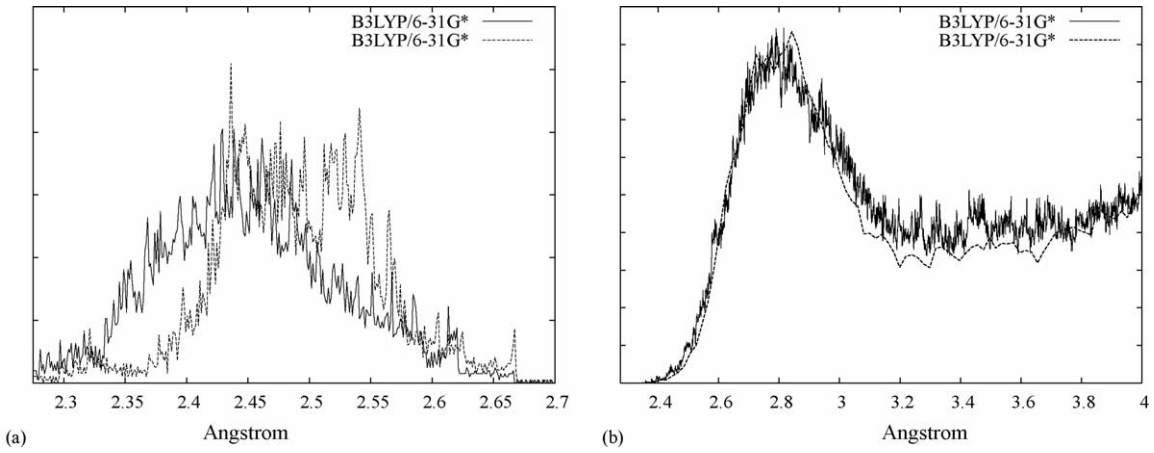

Fig. 4. Radial distribution function of the distance between (a) the most protonated oxygen and unprotonated oxygens, (b) the unprotonated oxygens, for the $H^+(H_2O)_{31}$ cluster. For (a), it is know that for Zundel ions ($H_5O_2^+$) this distance is about 2.45 Å and for the symmetric Eigen ions ($H_9O_4^+$), this distance is around 2.55 Å. Note that BLYP shows an equal probability of both ions being present; not the case for B3LYP. This aspect seems to directly translate into the faster hopping rate for BLYP functional seen in Fig. 2. See discussion for details. The behavior of the unprotonated state is similar for both functionals as seen in (b).

behave in a markedly different manner. Furthermore, since the B3LYP proton transfer rates are in closer agreement with those obtained from higher level correlated calculations [28] we are inclined to accept our B3LYP results. For the present application this is, however, not an issue, since both functionals provide qualitatively similar results, i.e., the proton is ejected in both cases. On parting, we add that radial distribution functions similar to B3LYP were obtained from the MS-EVB2 treatment of the 31-mer. MS-EVB2 was the method used in [48].

4. Conclusion

It is seen from our ADMP studies that the protonated species in a water cluster tends to reside on the surface rather than be completely solvated in the interior. Similar results have been found for negatively charged ions [68–71], however this has generally not been the case for positive charges [69–71]. The preferential behavior of the anions has been attributed to the local anisotropy of the structure of the water molecules surrounding the negative charge. In the present work we have confirmed our earlier result [48] where the H_3O^+ ion shows a propensity to reside on the surface of a cluster. This seemingly counter-intuitive result is explained based on the fluxional bonding topology of the protonated species, as stated in the introductory section of this paper. It is on this account that the H_3O^+ ion fundamentally differs from other positive and negative ions studied in [68–71] and the directionality of the hydrogen bond is the main factor here. Clearly, this directionality plays a very important role in our findings. Furthermore, the greater propensity of the hydronium to remain on the surface of the cluster, hints at a possible "hydrophobic" nature of the hydronium ion.

In addition to the above interesting observations we also found in the ADMP simulations that the well-known functionals B3LYP and BLYP provide quantitatively different mechanisms of the proton hop. While the BLYP functional supports a more delocalized (Eigen) state for the proton, the B3LYP functional prefers the more localized Zundel configuration. We attempt to explain this based on the possibility of greater electronic exchange interactions near the positively charged site.

Finally, we conclude that the second generation MS-EVB model provides qualitatively similar results as the ADMP method. It is especially interesting to note that the hydrogen bonding properties of the protonated oxygen in the MS-EVB calculations are qualitatively similar to those in the more rigorous B3LYP hybrid density functional.

Acknowledgments

This research was supported by the National Science Foundation (CHE-0317132) (GAV) and the Camille and Henry Dreyfus Foundation (SSI).

References

[1] T.S. Zwier, Science 304 (2004) 1119.
[2] J.-W. Shin, N.I. Hammer, E.G. Diken, M.A. Johnson, R.S. Walters, T.D. Jaeger, M.A. Duncan, R.A. Christie, K.D. Jordan, Science 304 (2004) 1137.
[3] M. Miyazaki, A. Fujii, T. Ebata, N. Mikami, Science 304 (2004) 1134.
[4] X.-D. Xiao, V. Vogel, Y.R. Shen, Chem. Phys. Lett. 163 (1989) 555.
[5] C. Radüge, V. Pflumio, Y.R. Shen, Chem. Phys. Lett. 274 (1997) 140.
[6] M. Okumura, L.I. Yeh, J.D. Myers, Y.T. Lee, J. Phys. Chem. 94 (1990) 3416.
[7] T.F. Magnera, D.E. David, J. Michl, Chem. Phys. Lett. 182 (1991) 363.
[8] X. Yang, X. Zhang, A.W. Castleman Jr., Int. J. Mass Spectrom. Ion Proc. 109 (1991) 339.
[9] S. Wei, Z. Shi, A.W. Castleman Jr., J. Chem. Phys. 94 (1991) 3268.
[10] U. Achatz, B.S. Fox, M.K. Beyer, V.E. Bondybey, J. Am. Chem. Soc. 123 (2001) 6151.
[11] S.-W. Lee, H. Cox, I.W.A. Goddard, J.L. Beauchamp, J. Am. Chem. Soc. 122 (2000) 9201.
[12] M. Meot-Ner (Mautner), S. Scheiner, W.O. Yu, J. Am. Chem. Soc. 120 (1998) 6980.
[13] N. Agmon, Chem. Phys. Lett. 244 (1995) 456.
[14] R.P. Bell, The Proton in Chemistry, Cornell University Press, Ithaca, NY, 1973.
[15] M. Eigen, L.D. Maeyer, Proc. R. Soc. Lond. Ser. A 247 (1958) 505.
[16] M. Eigen, Chem. Int. Ed. Engl. 3 (1964) 1.
[17] G. Zundel, in: P. Schuster, G. Zundel, C. Sandorfy (Eds.), The Hydrogen Bond-Recent Developments in Theory and Experiments. II. Structure and Spectroscopy, North-Holland, Amsterdam, 1976, p. 683.
[18] D. Eisenberg, W. Kauzman, The Structure and Properties of Water, Oxford University Press, Oxford, 1969.
[19] R.M. Lynden-Bell, J.C. Rasaiah, J. Chem. Phys. 105 (1996) 9266.
[20] J. Lobaugh, G.A. Voth, J. Chem. Phys. 104 (1996) 2056.
[21] R. Pomes, B. Roux, Biophys J. 71 (1996) 19.
[22] R. Pomes, B. Roux, J. Phys. Chem. 100 (1996) 2519.
[23] H. Decornez, K. Drukker, S. Hammes-Schiffer, J. Phys. Chem. A 103 (1999) 2891.
[24] M.L. Brewer, U.W. Schmitt, G.A. Voth, Biophys J. 80 (2001) 1691.
[25] C.J. Tsai, K.D. Jordon, Chem. Phys. Lett. 213 (1993) 181.
[26] S.S. Xantheas, J. Chem. Phys. 100 (1994) 7523.
[27] S.S. Xantheas, J. Chem. Phys. 102 (1995) 4505.
[28] S. Sadhukhan, D. Munoz, C. Adamo, G.E. Scuseria, Chem. Phys. Lett. 306 (1999) 83.
[29] Y. Xie, R.B. Remington, H.F. Schaefer, III, J. Chem. Phys. 101 (1994) 4878.
[30] L. Ojamae, I. Shavitt, S.J. Singer, Int. J. Quantum Chem., Quantum Chem. Symp. 29 (1995) 657.
[31] L. Ojamae, I. Shavitt, S.J. Singer, J. Chem. Phys. 109 (13) (1998) 5547.
[32] H.-P. Cheng, J. Phys. Chem. A 102 (1998) 6201.
[33] R.R. Sadeghi, H.-P. Cheng, J. Chem. Phys. 111 (1999) 2086.
[34] H.-P. Cheng, J.L. Krause, J. Chem. Phys. 107 (1997) 8461.
[35] D. Wei, D.R. Salahub, J. Chem. Phys. 106 (1997) 6086.
[36] E.S. Kryachko, Chem. Phys. Lett. 314 (1999) 353.
[37] M.E. Tuckerman, K. Laasonen, M. Sprik, M. Parrinello, J. Phys. Chem. 99 (1995) 5749.
[38] D. Marx, M.E. Tuckerman, J. Hutter, M. Parrinello, Nature 397 (1999) 601.
[39] A. Banerjee, R. Shepard, J. Simons, J. Chem. Phys. 73 (1980) 1814.
[40] A. Banerjee, A. Quigley, R.F. Frey, D. Johnson, J. Simons, J. Am. Chem. Soc. 109 (1987) 1038.
[41] P.M. Holland, A.W. Castleman Jr., J. Chem. Phys. 72 (1980) 5984.
[42] M.M. Teeter, Proc. Natl. Acad. Sci. U.S.A. 81 (1984) 6014.
[43] S. Neidle, H.M. Berman, H.S. Shieh, Nature 288 (1980) 129.

[44] L.A. Lipscomb, M.E. Peek, F.X. Zhou, J.A. Bertrand, D. VanDerveer, L.D. Williams, Biochemistry 33 (1994) 33.
[45] C. Tu, R.S. Rowlett, B.C. Tripp, J.G. Ferry, D.N. Silverman, Biochemistry 41 (2002) 15429.
[46] M.J. McEwan, L.F. Phillips, Chemistry of the Atmosphere, Eward Arnold, London, 1975.
[47] R.P. Wayne, Chemistry of the Atmosphere, Clarendon Press, Oxford, 1994.
[48] M.K. Petersen, S.S. Iyengar, T.J.F. Day, G.A. Voth, J. Phys. Chem. B 108 (2004) 14804.
[49] U.W. Schmitt, G.A. Voth, J. Chem. Phys. 111 (1999) 9361.
[50] T.J.F. Day, A.V. Soudachov, M. Cuma, U.W. Schmitt, G.A. Voth, J. Chem. Phys. 117 (2002) 5839.
[51] H.B. Schlegel, J.M. Millam, S.S. Iyengar, G.A. Voth, A.D. Daniels, G.E. Scuseria, M.J. Frisch, J. Chem. Phys. 114 (2001) 9758.
[52] S.S. Iyengar, H.B. Schlegel, J.M. Millam, G.A. Voth, G.E. Scuseria, M.J. Frisch, J. Chem. Phys. 115 (2001) 10291.
[53] H.B. Schlegel, S.S. Iyengar, X. Li, J.M. Millam, G.A. Voth, G.E. Scuseria, M.J. Frisch, J. Chem. Phys. 117 (2002) 8694.
[54] S.S. Iyengar, H.B. Schlegel, G.A. Voth, J.M. Millam, G.E. Scuseria, M.J. Frisch, Israel J. Chem. 42 (2002) 191.
[55] N. Rega, S.S. Iyengar, G.A. Voth, H.B. Schlegel, M.J. Frisch, J. Phys. Chem. B 108 (2004) 4210.
[56] S.S. Iyengar, H.B. Schlegel, G.A. Voth, J. Phys. Chem. A. 107 (2003) 7269.
[57] S.S. Iyengar, M.J. Frisch, J. Chem. Phys. 121 (2004) 5061.
[58] S.S. Iyengar, M.K. Petersen, T.J.F. Day, C.J. Burnham, G.A. Voth, J. Am. Chem. Soc., in preparation.
[59] A. Grossman, J. Morlet, SIAM J. Math. Anal. 15 (1984) 723.
[60] G. Strang, SIAM Rev. 31 (1989) 613.
[61] I. Daubechies, Ten Lectures in Wavelets, SIAM, 1992.
[62] G. Strang, T. Nguyen, Wavelets and Filter Banks, Wellesley-Cambridge Press, 1996.
[63] G.H. Golub, C.F. van Loan, Matrix Computations, The Johns Hopkins University Press, Baltimore, 1996.
[64] P. Pulay, Mol. Phys. 17 (1969) 197.
[65] F. Riesz, B. Sz -Nagy, Functional Analysis, Dover Publications Inc., New York, 1990.
[66] M.K. Petersen, S.S. Iyengar, T.J.F. Day, C.J. Burnham, G.A. Voth, Science, in preparation.
[67] M.J. Frisch, G.W. Trucks, H.B. Schlegel, G.E. Scuseria, M.A. Robb, J.R. Cheeseman, J.A. Montgomery Jr., T. Vreven, K.N. Kudin, J.C. Burant, J.M. Millam, S.S. Iyengar, J. Tomasi, V. Barone, B. Mennucci, M. Cossi, G. Scalmani, N. Rega, G.A. Petersson, H. Nakatsuji, M. Hada, M. Ehara, K. Toyota, R. Fukuda, J. Hasegawa, M. Ishida, T. Nakajima, Y. Honda, O. Kitao, H. Nakai, M. Klene, X. Li, J.E. Knox, H.P. Hratchian, J.B. Cross, C. Adamo, J. Jaramillo, R. Gomperts, R.E. Stratmann, O. Yazyev, A.J. Austin, R. Cammi, C. Pomelli, J.W. Ochterski, P.Y. Ayala, K. Morokuma, G.A. Voth, P. Salvador, J.J. Dannenberg, V.G. Zakrzewski, S. Dapprich, A.D. Daniels, M.C. Strain, O. Farkas, D.K. Malick, A.D. Rabuck, K. Raghavachari, J.B. Foresman, J.V. Ortiz, Q. Cui, A.G. Baboul, S. Clifford, J. Cioslowski, B.B. Stefanov, G. Liu, A. Liashenko, P. Piskorz, I. Komaromi, R.L. Martin, D.J. Fox, T. Keith, M.A. Al-Laham, C.Y. Peng, A. Nanayakkara, M. Challacombe, P.M.W. Gill, B. Johnson, W. Chen, M.W. Wong, C. Gonzalez, J.A. Pople, Gaussian 03, Revision b.02. Gaussian Inc., Pittsburgh, PA, 2003.
[68] D.J. Tobias, P. Jungwirth, M. Parrinello, J. Chem. Phys. 114 (2001) 7036.
[69] L. Perera, M.L. Berkowitz, J. Chem. Phys. 95 (1991) 1954.
[70] L. Perera, M.L. Berkowitz, J. Chem. Phys. 96 (1992) 8288.
[71] L. Perera, M.L. Berkowitz, J. Chem. Phys. 99 (1993) 4236.